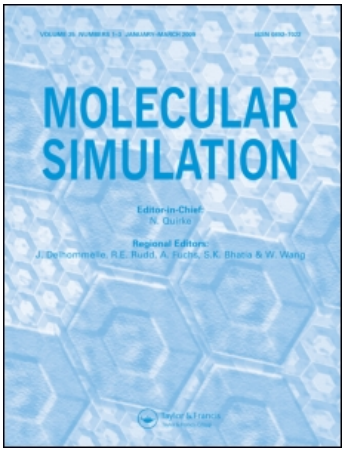

Molecular Simulation
Publication details, including instructions for authors and subscription information:
http://www.informaworld.com/smpp/title~content=t713644482

An atomistic analysis of incipient metal plasticity during tensile loading

R. S. McEntire[ab]; Y. -L. Shen[a]
[a] Department of Mechanical Engineering, University of New Mexico, Albuquerque, NM, USA [b] Sandia National Laboratories, Albuquerque, NM, USA

To cite this Article McEntire, R. S. and Shen, Y. -L.(2006) 'An atomistic analysis of incipient metal plasticity during tensile loading', Molecular Simulation, 32: 10, 857 — 867
To link to this Article: DOI: 10.1080/08927020600925789
URL: http://dx.doi.org/10.1080/08927020600925789

Molecular Simulation, Vol. 32, Nos. 10–11, 30 August–15 September 2006, 857–867

Taylor & Francis
Taylor & Francis Group

An atomistic analysis of incipient metal plasticity during tensile loading

R. S. McENTIRE†‡ and Y.-L. SHEN†*

†Department of Mechanical Engineering, University of New Mexico, Albuquerque, NM 87131, USA
‡Sandia National Laboratories, Albuquerque, NM 87185, USA

(Received February 2006; in final form March 2006)

Crystallographic slip at the beginning stages of plastic deformation is investigated via an atomistic (molecular statics) model. Attention is devoted to face-center-cubic metallic crystals in the form of a nanowire under uniaxial tensile loading. The simulation parameters employed in this work are such that dislocation slip behavior can be observed without the influence of surface stress and phase transformation. The incorporation of an initial embedded point defect in the model causes plastic deformation to be facilitated in a controlled manner. Two crystallographic orientations are studied, [7 $\overline{1}$0 $\overline{3}$] and [2 $\overline{1}$ 1], which result in, respectively, single slip and double slip at the onset of plastic yielding. Detailed mechanisms of dislocation evolution and their glide features are analyzed.

Keywords: Atomistic simulation; Plastic deformation; Crystal; Dislocation

1. Introduction

Atomistic simulations are being increasingly utilized for studying complicated microscopic features in crystalline solids. Traditionally, simulations of plastic defect mechanisms in crystals are best manifested by the nanoindentation [1–8] and crack tip [9–15] processes. Simulation of these problems causes nucleation and subsequent movement of dislocations that can provide insight into the localized nature of the deformation field and experimentally observed phenomena. The analysis of incipient plasticity during tensile stretching of a stand-alone crystal has received great attention in recent years, particularly for materials in the form of a nanowire [16–21]. For such small specimens with large surface-to-volume ratios, the surface energy is found to play a very significant role in affecting the mechanical response, leading to possible phase transformation, yield asymmetry, lattice reorientation, and the shape memory effect. Simulation studies have primarily focused on tensile loading along high-symmetry crystallographic directions including $<100>$, $<110>$ and $<111>$. The present work, however, concerns loading along orientations with relatively low-symmetry. In particular, our attention is devoted to the analysis of dislocation slip activity at the beginning stages of plastic deformation. We consider two crystal orientations which give rise to "single slip" and "double slip" when plastic yielding occurs. Furthermore, in previous 2D atomistic studies we have used an embedded initial point defect for triggering plasticity events at a prescribed location in the model, a convenient feature for computational analyses [22,23]. The applicability of this approach in a 3D crystal is tested in the present work. The correlation between the overall mechanical response and atomistic deformation features is also investigated.

2. Computational model

Figure 1 shows a schematic of the model setup. Atoms are packed into an FCC crystal, and the specimen takes the form of a rectangular bar to be subject to tensile stretching. We consider two cases of tensile loading orientations: [7 $\overline{1}$0 $\overline{3}$] and [2 $\overline{1}$ 1]. The first (relatively high-index) orientation is arbitrarily chosen to ensure single slip when the first slip is activated. (The slip system is (1 $\overline{1}$ 1)[0 1 1] with a maximum Schmid factor of 0.4702.) The second orientation, with two slip systems, (1 1 1)[$\overline{1}$ 1 0] and ($\overline{1}$ 1 1)[1 0 1], each having the same greatest Schmid factor

*Corresponding author. Email: shenyl@me.unm.edu

Molecular Simulation
ISSN 0892-7022 print/ISSN 1029-0435 online © 2006 Taylor & Francis
http://www.tandf.co.uk/journals
DOI: 10.1080/08927020600925789

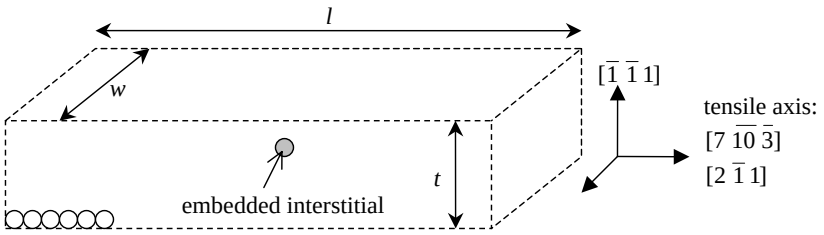

Figure 1. Schematic of the model geometry and crystal orientation.

(0.4082), should in principle give rise to double slip when plasticity commences. The model dimensions are characterized by the outermost edges of the atomic spheres in the three directions: $l = 128.0$ Å, $w = 24.73$ Å, $t = 17.19$ Å for the $[7\,\overline{1}0\,\overline{3}]$ loading and $l = 108.98$ Å, $w = 28.16$ Å, $t = 17.19$ Å for the $[2\,\overline{1}\,1]$ loading. Note the thickness (t) direction is fixed to be $[\overline{1}\,\overline{1}\,1]$ in both models. The Morse interatomic potential is used with parameters

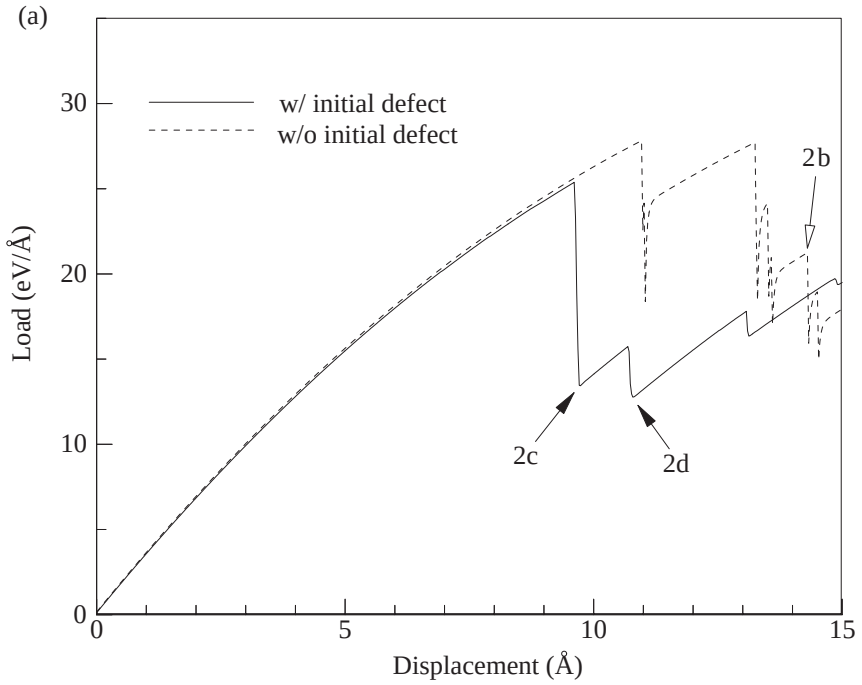

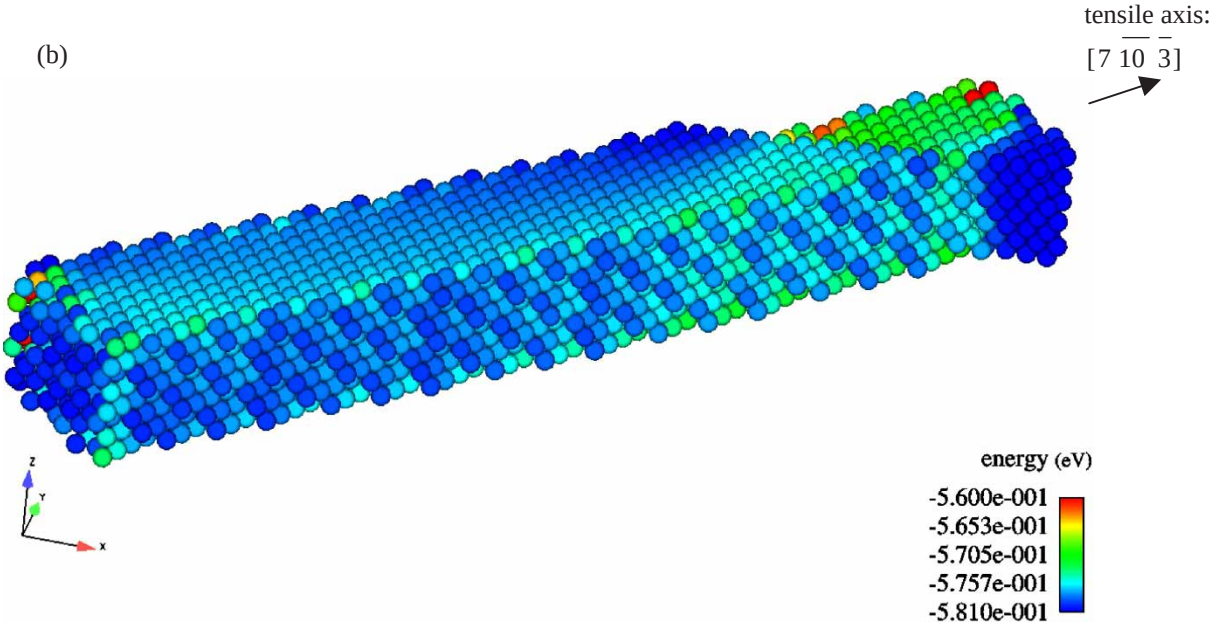

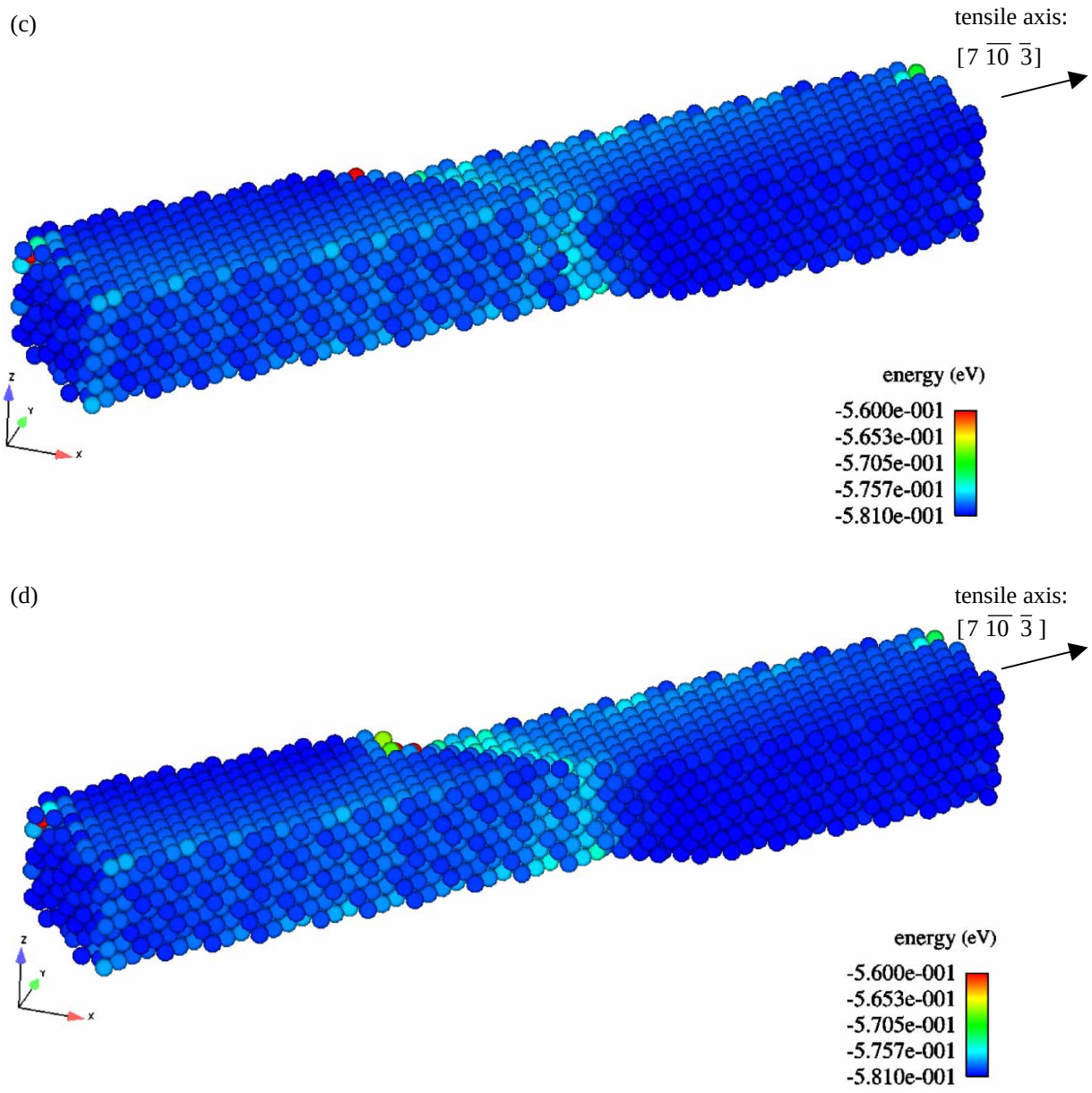

Figure 2. (a) Simulated overall tensile load-displacement curves for the case of [7 $\overline{10}$ $\overline{3}$] loading. (b)–(d) Snapshots of atomic positions corresponding to points 2b–2d, respectively, along the load-displacement curves shown in (a).

determined by fitting the potential equation to experimental data for the close-packed equilibrium atomic spacing (2.56 Å), cohesive energy (3.48 eV) and bulk modulus (134 GPa) of copper featuring near-neighbor interactions [22–24]. In particular, we consider an atomic interaction range of $1.325r_0$, where r_0 is the equilibrium atomic spacing in the unstressed state. Note this range is less than the distance between an internal atom and its second-nearest neighbors in the FCC structure (second-nearest neighbors are $1.414r_0$ away). Although this is a simplification from realistic copper, it serves to suppress all surface stress effects and phase transformation [25], which enables focal examination of dislocation slip behavior during plastic yielding. As schematically shown in figure 1, an initial point defect in the form of a self-interstitial is placed at the geometrical center of the model and allowed to equilibrate with its surrounding atoms before the loading steps commence. For comparison purposes, simulations without the initial defect in the model are also performed.

The molecular statics simulation is carried out by prescribing a small displacement in the tensile direction on the end atoms at each loading step. Lateral displacement of these end atoms is not allowed. Atoms on the face opposite to the pulling end are fixed. The side boundary atoms in the rest of the specimen are not constrained. In response to each prescribed loading step all atomic points are allowed to iteratively reach their new equilibrium positions. The overall load is calculated by summing the force components along the tensile direction pertaining to the atoms where the displacement is prescribed.

3. Results and discussion

3.1 *The* [7 $\overline{1}$0 $\bar{3}$] *loading*

Figure 2(a) shows the simulated overall load-displacement curves in the case of [7 $\overline{1}$0 $\bar{3}$] loading with and without the initial defect incorporated. Attention is confined to the beginning stages of plastic deformation. Since, the deformation modeling is displacement-controlled, any significant slip and formation of surface steps (signifying permanent shape change of the crystal) will be associated with a sharp reduction in overall load along the load-displacement curve, as illustrated in previous 2D simulations [22,23]. This is also the case in the present 3D analysis. Three snapshots of atomic configurations

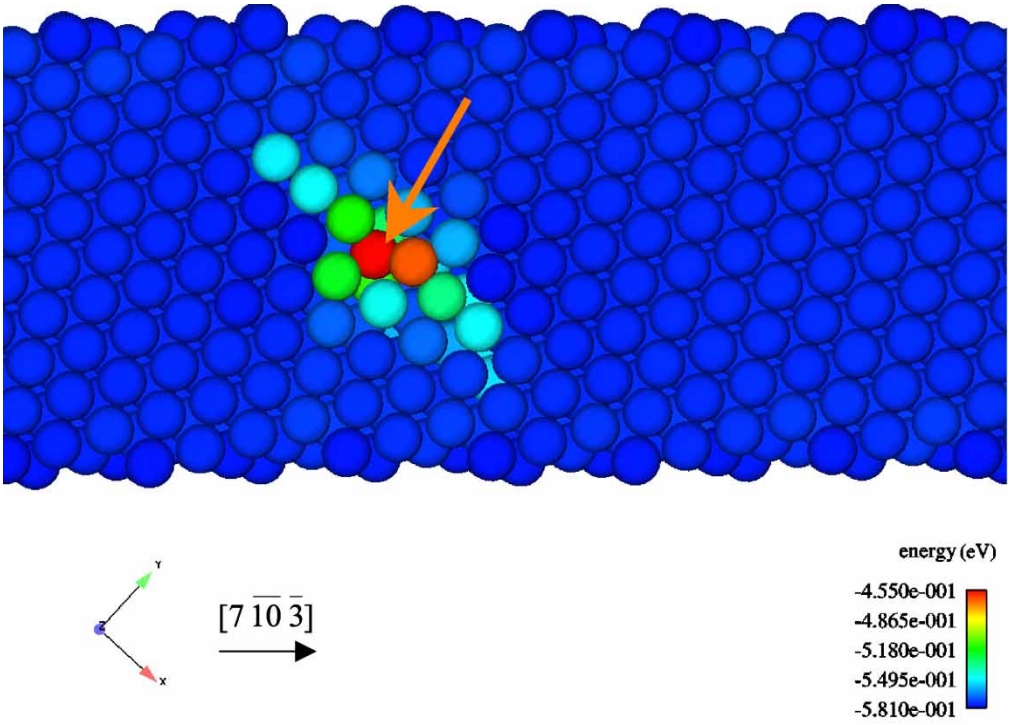

(a)

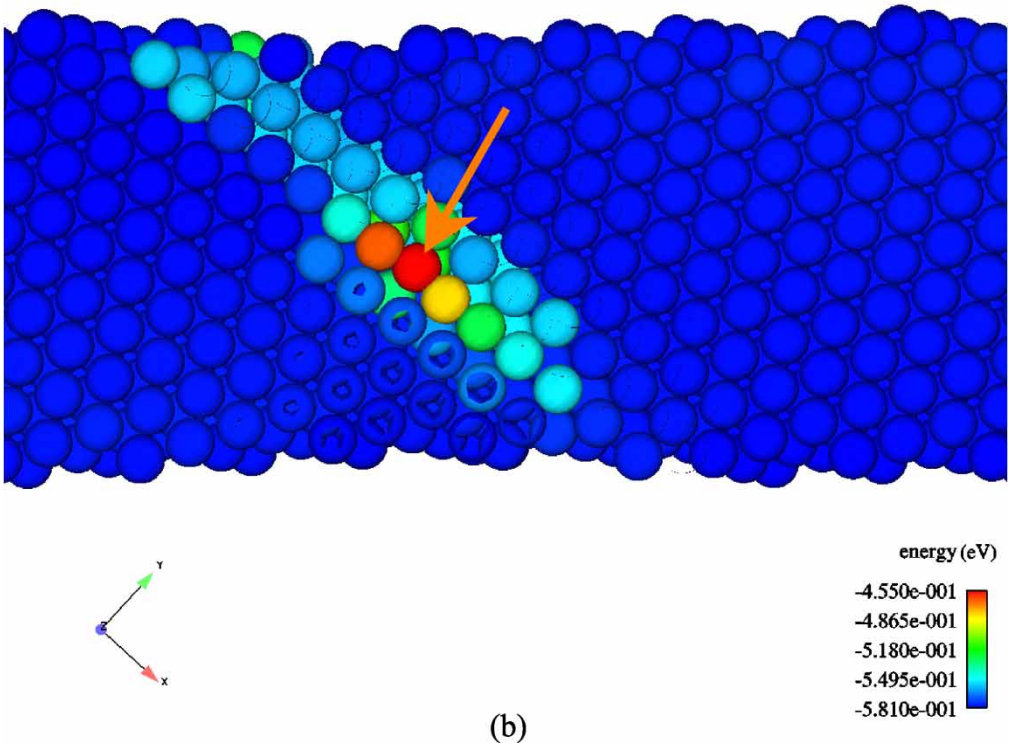

(b)

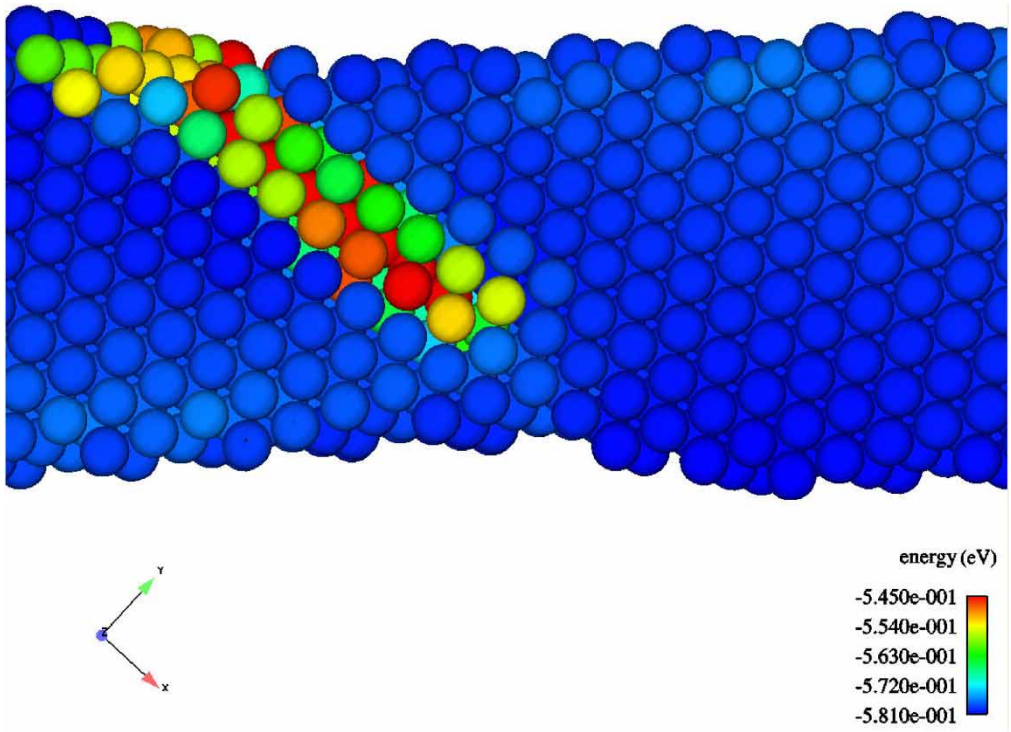

(c)

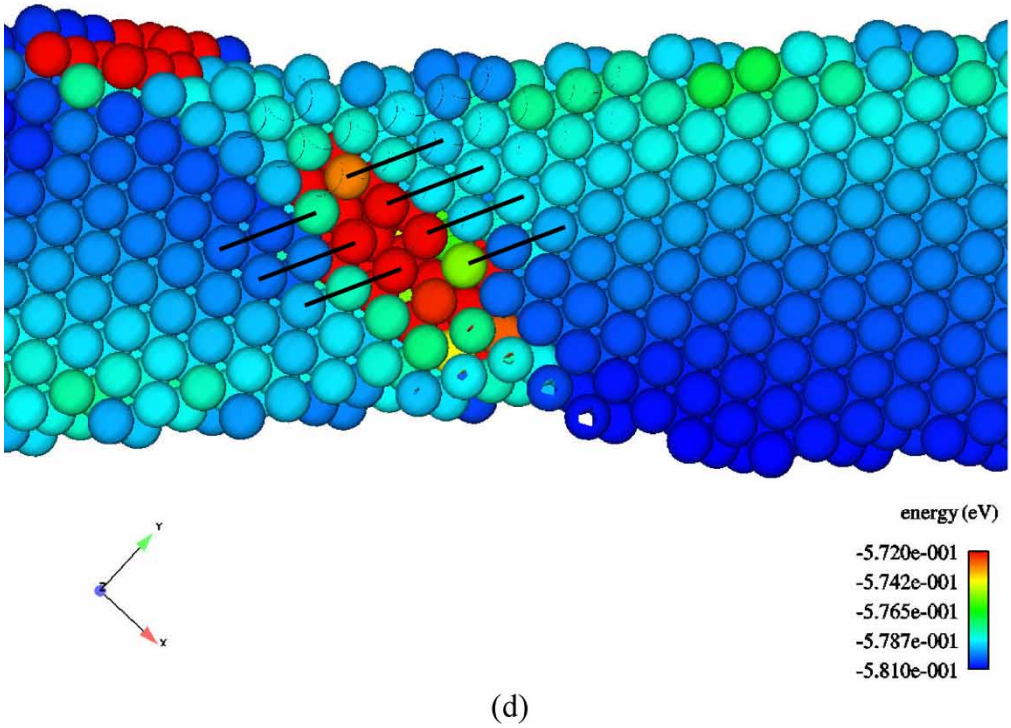

(d)

Figure 3. (a) and (b) Snapshots of atomic arrangement along an internal section of $(\bar{1}\,\bar{1}\,1)$ plane passing through the initial interstitial atom (highlighted by arrow) shortly before the first reduction of overall load during tensile stretching along $[7\,\overline{10}\,\bar{3}]$. (c) and (d) Snapshots of atomic arrangement along an internal section of $(\bar{1}\,\bar{1}\,1)$ plane, one atomic layer above those in (a) and (b), during the first reduction of overall load during tensile stretching along $[7\,\overline{10}\,\bar{3}]$.

are presented in figure 2(b)–(d), which correspond to the points 2b–d, respectively, labeled along the load-displacement histories in figure 2(a). The atoms are color-coded to display their relative energy state in the deformed configuration. It can be seen in figure 2(b) that, without the initial defect, slip along the $(1\,\bar{1}\,1)[0\,1\,1]$ primary system (with the greatest Schmid factor) has occurred. However, it was initiated at the corner of the specimen. Continued deformation will force a strong elastic distortion of the crystal, due to the constraining of the end atoms which

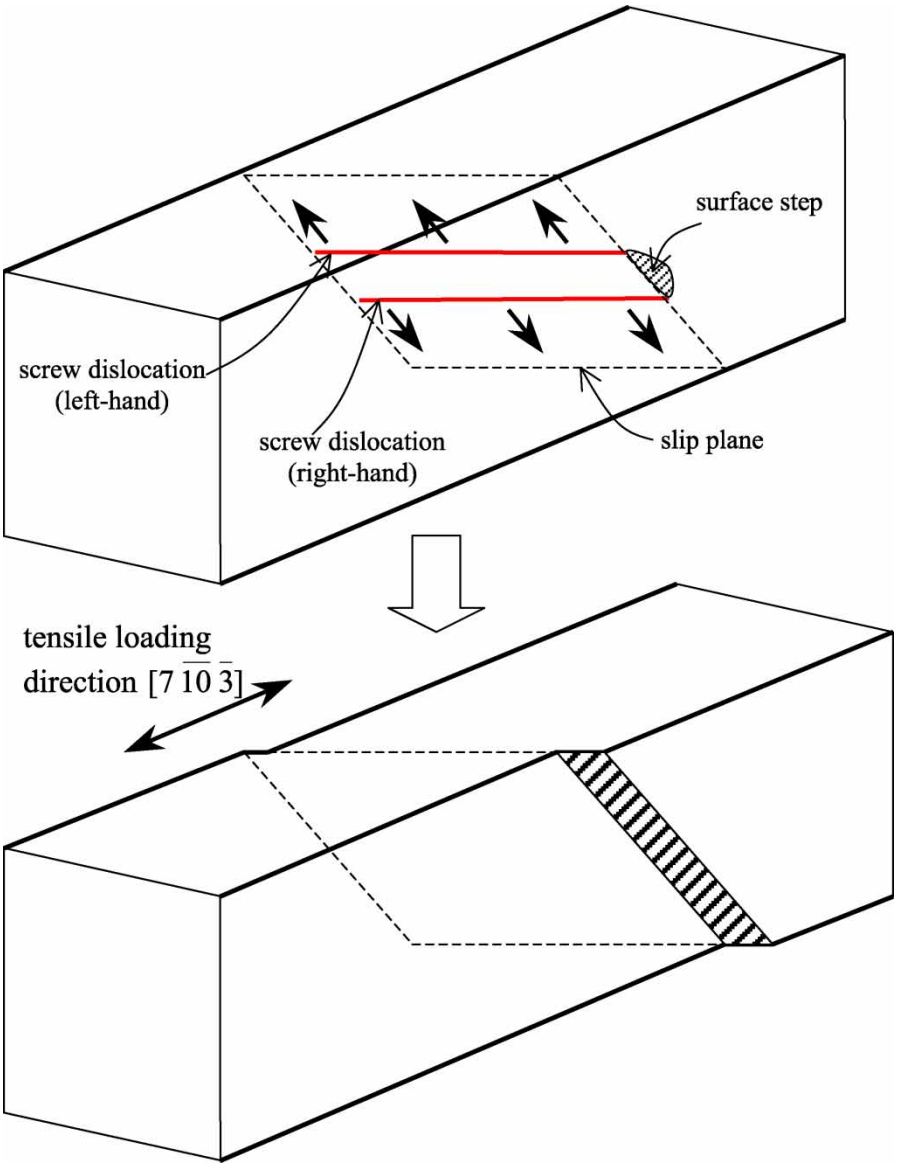

Figure 4. Schematics illustrating the dislocation slip mechanism and crystal shape change at the beginning stages of plastic deformation during the [7 $\bar{1}$0 $\bar{3}$] loading.

prevents the conjugate slip system from being activated (not shown here).

Figure 2(c),(d) show the atomic configurations at the bottom points of the first two abrupt reductions in overall load, for the case with an initial defect. It is seen that plastic yielding is now initiated from the center of the specimen. The primary slip system is also (1 $\bar{1}$ 1)[0 1 1]. Each load reduction is associated with the creation of slip steps along the slip direction. The observed behavior clearly suggests the capability of this approach in forcing the slip to be activated at a specified location. We have also observed that, with subsequent deformation (and thus lattice rotation), the conjugate slip system was activated leading to a symmetric deformation pattern until final fracture. This, however, is beyond the scope of the present report.

The detailed mechanism of how the initial point defect evolves into the dislocation slip operation deserves attention. Figure 3(a) shows the top view (viewing direction along [$\bar{1}$ $\bar{1}$ 1]) of an internal section of the ($\bar{1}$ $\bar{1}$ 1) plane containing the initial interstitial atom, when the specimen is deformed to shortly before the first overall load reduction shown in figure 2(a). The initial interstitial atom is highlighted by an arrow in the figure. At this moment due to the elastic deformation of the crystal, the interstitial atom (initially occupying an octahedral site) is being accommodated by its surrounding atoms. At the next moment, figure 3(b), the atom is seen aligned with its neighbors along the close-packed [0 1 1] direction. A linear array of atoms having high energy states can be seen. Figure 3(c),(d) show another internal section, parallel to, but one atomic layer above, those in 3(a) and

(b), during the first overall load reduction. Several parallel lines along [1 $\bar{1}$ 0] were drawn in figure 3(d), illustrating staggered arrays across the "discontinuity" which is a screw dislocation along the slip direction [0 1 1]. The formation of screw dislocation can also be demonstrated by the Burgers circuit operation on the side surface of the specimen (not shown here).

The incipient plastic deformation process can now be depicted by the schematics in figure 4, where the dislocation slip mechanism and the resulting crystal shape change are shown. Upon the "absorption" of the interstitial into a line of atoms along the maximum shear direction, a small bulge at the end of the atomic line on the side surface becomes the starting point for forming the surface step, from which a pair of screw dislocations evolves. The slip of these dislocations leads to plastic yielding of the crystal.

3.2 The [2 $\bar{1}$ 1] *loading*

We now consider the case of tensile loading along the [2 $\bar{1}$ 1] orientation. Figure 5(a) shows the simulated overall load-displacement curves. If there is no initial defect in the model, plastic yielding does not occur at all. Following the elastic response, the model fails in a strictly brittle way (with the load dropping straight down to zero seen in figure 5(a)). The fact that there is no plastic deformation starting from the specimen corner, as opposed to the

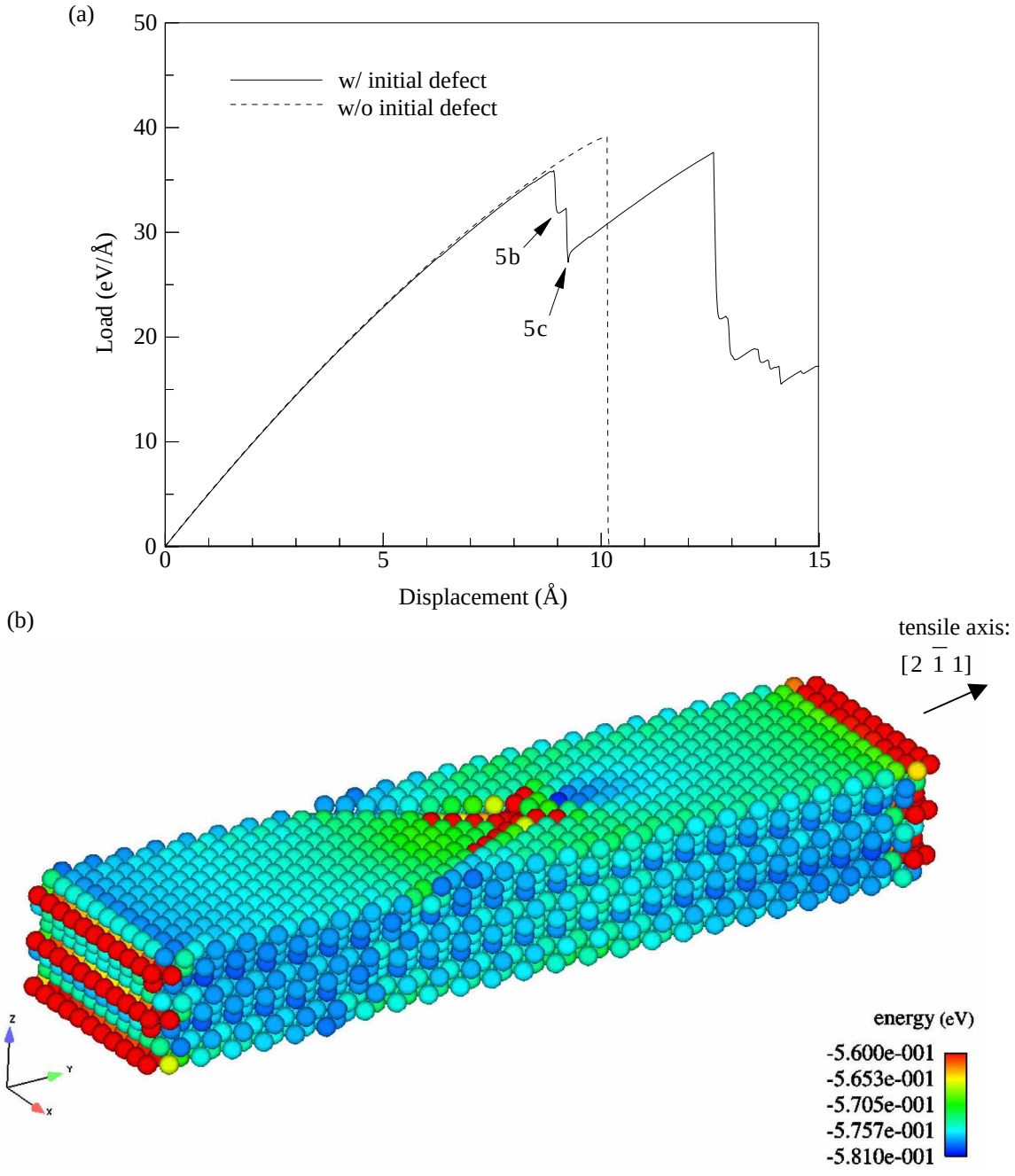

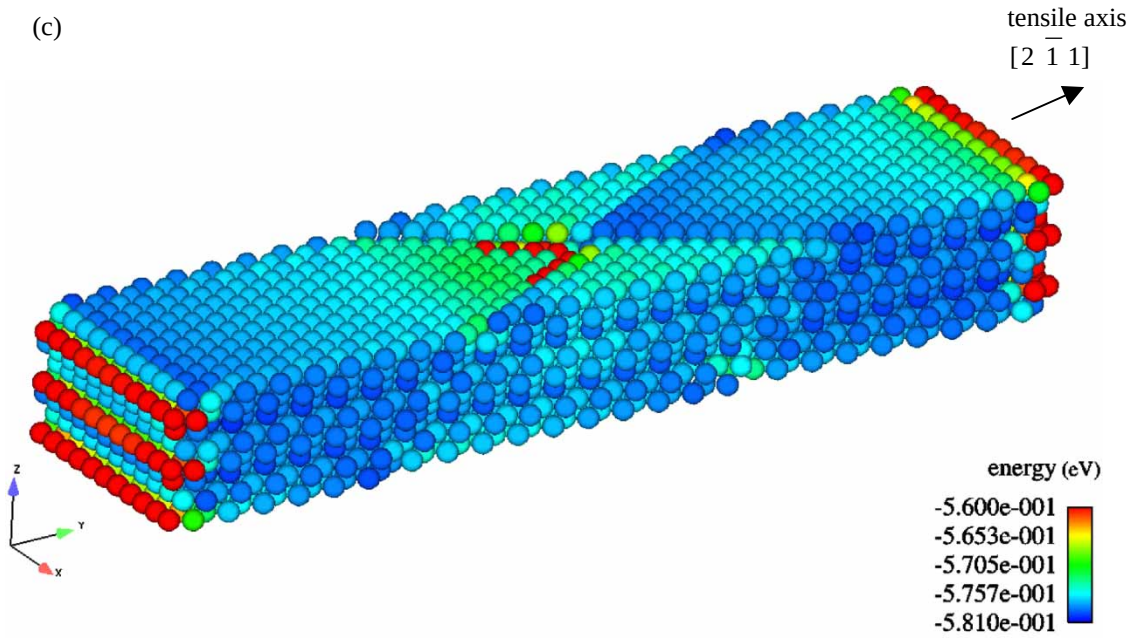

Figure 5. (a) Simulated overall tensile load-displacement curves for the case of [2 $\bar{1}$ 1] loading. (b) and (c) Snapshots of atomic positions corresponding to points 5b and 5c, respectively, along the load-displacement curves shown in (a).

previous [7 $\overline{10}$ $\bar{3}$] loading, may be due to the lower magnitude of the Schimd factor in the present situation: a higher tensile stress will be needed to activate slip, therefore, the atomic bond breaking occurs before such stress is reached.

Contrarily, with the incorporation of an initial defect, extensive plastic deformation initiated from the defect site can be observed. Figure 5(b),(c) show the snapshots of atomic configurations corresponding to points 5b and 5c, respectively, labeled in figure 5(a). It is evident that double slip occurs. However, slip does not occur along the systems (1 1 1)[$\bar{1}$ 1 0] and ($\bar{1}$ 1 1)[1 0 1] with the maximum Schmid factor. Instead, the activated slip systems are (1 1 1)[0 $\bar{1}$ 1] and ($\bar{1}$ 1 1)[0 $\bar{1}$ 1] with a Schmid factor of 0.2722. The reason for this will be discussed below. Note the two slip systems have a common slip direction [0 $\bar{1}$ 1]. At the end of the first load reduction, figure 5(b), "v" shaped surface steps which are the slip traces of these two operating systems are clearly visible. After a brief elastic period, a second load reduction occurs with the same two slip systems operating, which causes the propagation of the existing slip traces, figure 5(c).

We now discuss the atomistic processes leading to the observed incipient plasticity. Figure 6(a) shows a snapshot of internal atomic positions along a center cut passing through the initial point defect, with the horizontal and vertical directions parallel to, respectively, the tensile axis [2 $\bar{1}$ 1] and the specimen thickness direction [$\bar{1}$ $\bar{1}$ 1], when the crystal is still under elastic deformation with an applied displacement of about 6.8 Å. At this stage the initial interstitial has joined a line of atoms along the [0 $\bar{1}$ 1] direction, as revealed by the high-energy atoms in figure 6(a). This crowded line of atoms serves to form a small bulge on the top and bottom surfaces of the specimen upon further deformation, which in turn generates a pair of screw dislocations (see figure 7 below). Plastic yielding occurs as the two screw dislocations, originated from the same line, slip along two different but symmetrically oriented slip planes. Figure 6(b) shows an external view of crystal during the first load reduction, with the two screw dislocations discernible gliding toward the side surfaces of the specimen. The entire process is summarized by the schematics shown in figure 7.

The fact that the two activated slip systems do not correspond to those of the maximum Schmid factor is apparently related to the dislocation nucleation process. In the present analysis, the source of the screw dislocation dipole is the line of atoms (after the inclusion of the interstitial) along [0 $\bar{1}$ 1], which serves as the common slip direction for the two activated systems (1 1 1)[0 $\bar{1}$ 1] and ($\bar{1}$ 1 1)[0 $\bar{1}$ 1] (figure 7). Therefore, the two screw dislocations can evenly slip out along two symmetrically oriented planes and form the "v" shaped slip steps. If the double slip were to occur along the slip systems with the greatest Schmid factor, (1 1 1)[$\bar{1}$ 1 0] and ($\bar{1}$ 1 1)[1 0 1], two pairs of dislocations would be required because of the two different slip directions (figure 7). The present model setup does not favor this form of slip operation. It is noted that the Schmid law is predicated upon the situation where sufficient sources of mobile dislocations exist, typically for large (micron-sized or above) crystals. The current analysis suggests that, in nanowire specimens with very limited defect source, when slip occurs the slip systems with the greatest Schmid factor may not be the first to be activated.

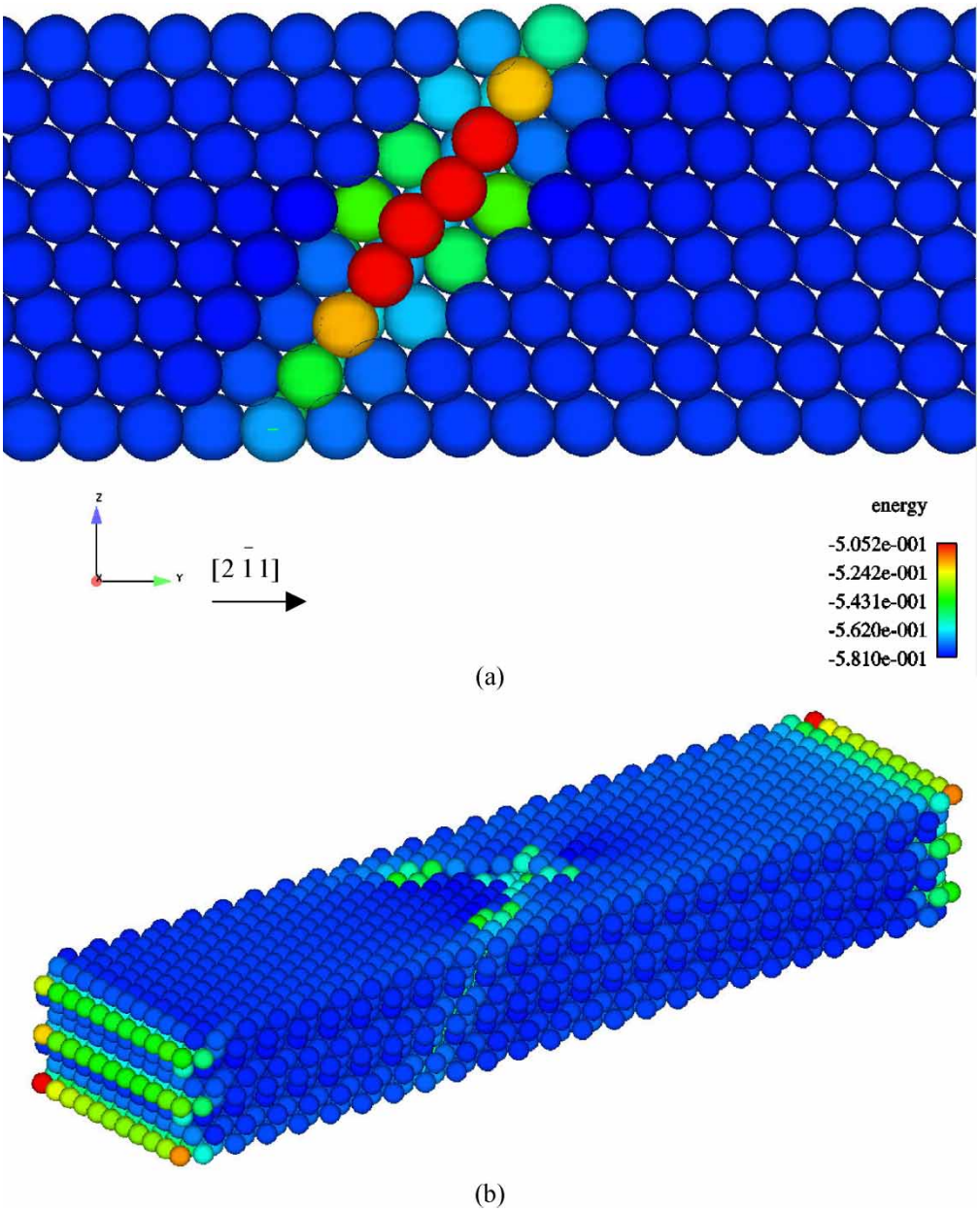

Figure 6. (a) Snapshot of atomic positions showing the accommodation of the initial interstitial atom into a line of close-packed atoms in the [0 $\bar{1}$ 1] direction. In this figure the horizontal direction is in the tensile axis [2 $\bar{1}$ 1] and the vertical direction is parallel to the specimen thickness direction [$\bar{1}$ $\bar{1}$ 1]. (b) Snapshot of external atomic configuration during the first overall load reduction (plastic yielding) of the specimen. Two screw dislocations are in the process of gliding toward the side surfaces.

3.3 Further discussion

In this study, we have used a molecular statics simulation technique to analyze uniaxial tensile loading of copper nanowire along the [7 $\overline{1}$0 $\bar{3}$] and [2 $\bar{1}$ 1] orientations and the dislocation slip response at the onset of plastic deformation. It has been argued, on the basis of comparison studies using the Lennard–Jones or Morse pair potentials and the many-body embedded atom potential [26,27], that while simulations involving only pair potentials generally yield brittle behavior, ductile materials *must* be described with a many-body potential [28,29]. In the present study, we have illustrated that, with the incorporation of an initial point defect, the employment of a pairwise interatomic potential is able to render a ductile behavior. In the previous 2D simulations applying the same technique [22,23,30], the initial point defect was observed to evolve into a pair of edge dislocations with opposite senses. In the present 3D study, the formation of two opposite screw dislocations is seen. In addition, both single and double slips can be facilitated with the qualitatively similar mechanism of dislocation emission. This is believed to be a useful simulation methodology to induce local plasticity in a controlled manner, which is of particular interest for studying the interaction between dislocations, and between a dislocation and other defects

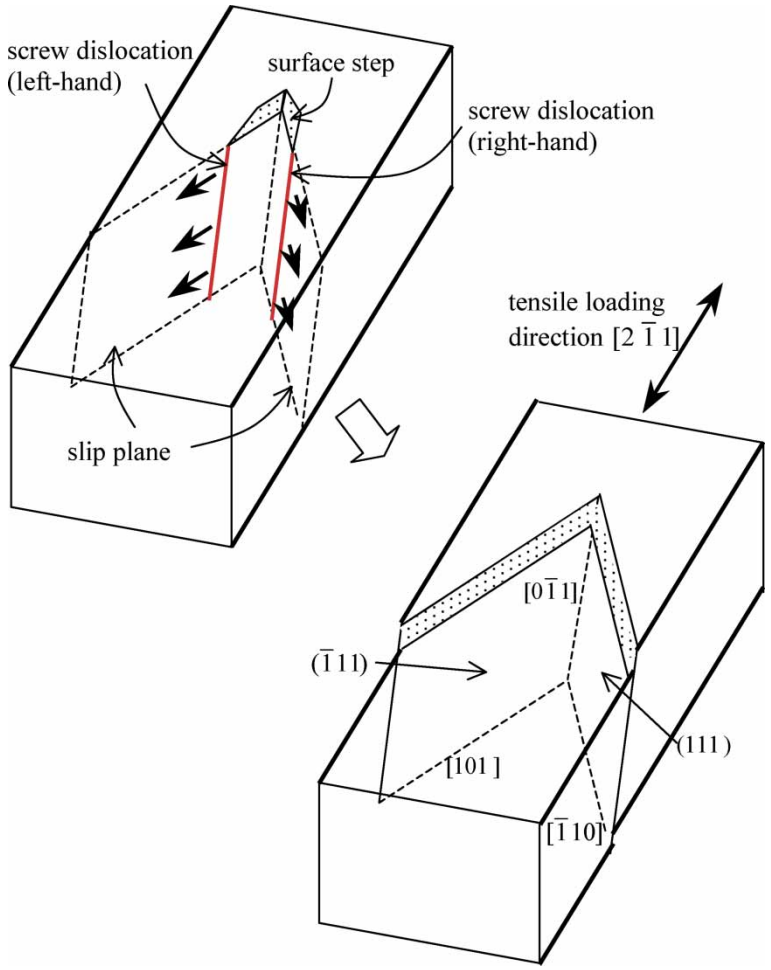

Figure 7. Schematics illustrating the dislocation slip mechanism and crystal shape change at the beginning stages of plastic deformation during the [2 $\bar{1}$ 1] loading.

such as grain boundaries, interfaces and inclusion particles.

Another implication of the present results, which may be of fundamental importance, is that an existing point defect in the crystal can serve as a source for dislocation nucleation during deformation. Although this study follows previous 2D simulations by making use of a self-interstitial atom, in actual materials vacancies are a more common form of point defects. The effect of vacancies in this type of atomistic simulation is worthy of further investigation.

4. Conclusions

We have carried out atomistic simulations of uniaxial tensile loading of an FCC metallic crystal in the form of a nanowire, focusing on incipient plastic yielding. The technique of embedding an initial point defect in the model was utilized. With this treatment, the use of a pair potential is seen to be able to yield a ductile behavior, avoiding brittle fracture or the boundary effect. This is believed to be a useful methodology for computationally studying the interaction between dislocations and other microstructural features in the crystals. For the purpose of gaining fundamental insight, the choice of interatomic potential parameters is such that dislocation slip is the favorable plastic deformation mechanism. Detailed analyses of atomic configurations revealed that, as the deformation progresses, the initial interstitial atom was gradually accommodated by a line of atoms along a close-packed direction, leading to a geometric condition favoring the formation of a pair of screw dislocations. In the case of [7 $\overline{10}$ $\bar{3}$] loading, plastic yielding occurs as a result of dislocation glide along the slip system with the maximum Schmid factor. In the case of [2 $\bar{1}$ 1] loading, double slip prevails with the two screw dislocations, originated along the same slip direction, gliding along two symmetric slip planes. In the latter case, the two active slip systems do not correspond to those with the greatest Schmid factor, owing to the unique form of dislocation nucleation in the model. This suggests that in physically small metallic specimens such as nanowires, the dislocation slip behavior, if present, will depend on the actual dislocation source and may not follow the Schmid law in a quantitative manner.

References

[1] C.L. Kelchner, S.J. Plimpton, J.C. Hamilton. Dislocation nucleation and defect structure during surface indentation. *Phys. Rev. B*, **58**, 11085 (1998).

[2] E.B. Tadmore, R. Miller, R. Phillips, M. Ortiz. Nanoindentation and incipient plasticity. *J. Mater. Res.*, **14**, 2233 (1999).

[3] K.J. Van Vliet, J. Li, T. Zhu, S. Yip, S. Suresh. Quantifying the early stages of plasticity through nanoscale experiments and simulations. *Phys. Rev. B*, **67**, 104105 (2003).

[4] O. Rodriguez de la Fuente, J.A. Zimmerman, M.A. Gonzalez, J. de la Figuera, J.C. Hamilton, W.W. Pai, J.M. Rojo. Dislocation emission around nanoindentations on a (0 0 1) fcc metal surface studied by scanning tunneling microscopy and atomistic simulations. *Phys. Rev. Lett.*, **88**, 036101 (2002).

[5] D. Feichtinger, P.M. Derlet, H. Van Swygenhoven. Atomistic simulations of spherical indentations in nanocrystalline gold. *Phys. Rev. B*, **67**, 024113 (2003).

[6] E.T. Lilleodden, J.A. Zimmerman, S.M. Foiles, W.D. Nix. Atomistic simulations of elastic deformation and dislocation nucleation during nanoindentation. *J. Mech. Phys. Solids*, **51**, 901 (2003).

[7] J.D. Schall, D.W. Brenner. Atomistic simulation of the influence of pre-existing stress on the interpretation of nanoindentation data. *J. Mater. Res.*, **19**, 3172 (2004).

[8] R.W. Leger, Y.-L. Shen, T.A. Khraishi. Defect nucleation during nanoindentation: an atomistic analysis. *J. Comput. Theor. Nanosci.*, **1**, 261 (2004).

[9] B. deCelis, A.S. Argon, S. Yip. Molecular dynamics simulation of crack tip processes in alpha-iron and copper. *J. Appl. Phys.*, **54**, 4864 (1983).

[10] E.Y. Baiguzin, A.I. Melker, A.I. Mikhailin. Atomic mechanisms of fracture nucleation and fracture development in two-dimensional crystals in thermodynamic equilibrium. 1. One-phase systems. *Phys. Status Solidi. A*, **108**, 205 (1988).

[11] M. Doyama. Simulation of plastic deformation of small iron and copper single crystals. *Nucl. Instrum. Methods Phys. Res. B*, **102**, 107 (1995).

[12] S.J. Zhou, D.M. Beazley, P.S. Lomdahl, B.L. Holian. Large-scale molecular dynamics simulations of three-dimensional ductile failure. *Phys. Rev. Lett.*, **78**, 479 (1997).

[13] D. Farkas. Atomistic studies of intrinsic crack-tip plasticity. *MRS Bull.*, **25**(5), 35 (2000).

[14] M. Ortiz, A.M. Cuitino, J. Knap, M. Koslowski. Mixed atomistic continuum models of material behavior: the art of transcending atomistics and informing continua. *MRS Bull.*, **26**(3), 216 (2001).

[15] J.G. Swadener, M.I. Baskes, M. Nastasi. Molecular dynamics simulation of brittle fracture in silicon. *Phys. Rev. Lett.*, **89**, 085503 (2002).

[16] J.-W. Kang, H.-J. Hwang. Mechanical deformation study of copper nanowire using atomistic simulation. *Nanotechnology*, **12**, 295 (2001).

[17] J. Diao, K. Gall, M.L. Dunn, A. Zimmerman. Atomistic simulation of the yielding of gold nanowire. *Acta Mater.*, **54**, 643 (2006).

[18] W. Liang, M. Zhou, F. Ke. Shape memory effect in Cu nanowires. *Nano Lett.*, **5**, 2039 (2005).

[19] J. Wang, H. Huang. Novel deformation mechanism of twinned nanowires. *Appl. Phys. Lett.*, **88**, 203112 (2006).

[20] J. Diao, K. Gall, L. Dunn. Yield strength asymmetry in metal nanowires. *Nano Lett.*, **4**, 1863 (2004).

[21] H.S. Park, A. Zimmerman. Modeling inelasticity and failure in gold nanowires. *Phys. Rev. B*, **72**, 054106 (2005).

[22] M. Popova, Y.-L. Shen, T.A. Khraishi. Atomistic simulation of dislocation interactions in a model crystal subjected to shear. *Mol. Simul.*, **31**, 1043 (2005).

[23] M. Popova, L. Shen. Interaction between a dislocation and a nano-scale penetrable particle: a model atomistic study. *J. Comput. Theor. Nanosci.*, **3**, 448 (2006).

[24] R. Phillips. *Defects and Microstructures—Modeling Across Scales*, p. 206, Cambridge University Press, Cambridge (2001).

[25] R.S. McEntire, Y.-L. Shen. Atomistic analysis of crystal plasticity in copper nanowire. In *Mechanics of Nanoscale Materials and Devices*, Mater. Res. Soc. Symp. Proc., A. Misra, J.P. Sullivan, H. Huang, K. Lu, S. Asif (Eds.), (2006), paper number Z2.4.

[26] B.L. Holian, A.F. Voter, N.J. Wagner, R.J. Ravelo, S.P. Chen, W.G. Hoover, C.G. Hoover, J.E. Hammerberg, T.D. Dontje. Effects of pairwise versus many-body forces on high-stress plastic deformation. *Phys. Rev. A*, **43**, 2655 (1991).

[27] N.J. Wagner, B.L. Holian, A.F. Voter. Molecular dynamics simulations of two-dimensional materials at high strain rates. *Phys. Rev. A*, **45**, 8457 (1992).

[28] P. Heino, H. Hakkinen, K. Kaski. Molecular dynamics study of mechanical properties of copper. *Europhys. Lett.*, **41**, 273 (1998).

[29] P. Heino, H. Hakkinen, K. Kaski. Molecular dynamics study of copper with defects under strain. *Phys. Rev. B*, **58**, 641 (1998).

[30] Y.-L. Shen. Strength and interface-constrained plasticity in thin metal films. *J. Mater. Res.*, **18**, 2281 (2003).